Environmental Science
Water Research & Technology

ROYAL SOCIETY OF CHEMISTRY

PAPER

View Article Online
View Journal | View Issue

Cite this: *Environ. Sci.: Water Res. Technol.*, 2020, **6**, 1638

Photocatalytic reductive defluorination of perfluorooctanoic acid in water under visible light irradiation: the role of electron donor†

Wanjun Wang, Yu Chen, Guiying Li, Wenquan Gu and Taicheng An *

Received 7th March 2020,
Accepted 6th April 2020

DOI: 10.1039/d0ew00205d

rsc.li/es-water

The development of efficient technology for perfluorooctanoic acid (PFOA) treatment has prompted much attention in water environmental fields, due to its global distribution and threats to ecosystems. In this study, a new method for reductive defluorination of PFOA under visible light (VL) was established by using Pt–Bi_2O_4 as a photocatalyst and KI as an electron donor. The defluorination process in water was found to occur *via* a photocatalytic reductive pathway, in which the photo-generated e^- played the dominant role. The Pt served as a co-catalyst to trap the photo-generated e^-, while KI could trap photo-generated h^+ to suppress the undesired e^-–h^+ recombination, which cooperatively enhanced the defluorination efficiency. Along with PFOA reduction, very limited amounts of short-chain perfluorocarboxylic acid intermediates were generated, all of which could be further degraded to inorganic ions, and the total recovery of fluorine could reach 99% after 6 h of irradiation. The system also possesses high photostability, since the photocatalyst surface remained clean during the degradation. Finally, a decomposition pathway of stepwise removal of CF_2 units was proposed in detail. As a proof-of-concept, the VL/Pt–Bi_2O_4/KI system not only shows potential for sustainable and "green" removal of PFOA in water, but may also find applications in the treatment of various refractory organic pollutants in water using solar energy.

Water impact

Perfluorooctanoic acid (PFOA) as a persistent organic pollutant has aroused increasing concern in water pollution. The present study provides a new method for reductive defluorination of PFOA under visible light by using Pt–Bi_2O_4 as a photocatalyst and KI as an electron donor. This work provides a basis for sustainable and "green" treatment of PFOA and other refractory organic pollutants using solar energy.

1. Introduction

Perfluorooctanoic acid (PFOA) has a great variety of industrial applications, including emulsifying agents, protective coatings, and fire retardants.[1] Due to its widespread utilization, it has been detected in various environmental media including surface water with concentrations up to the ng L^{-1} level,[2] wildlife and even humans.[3,4] The bioaccumulation of PFOA and its toxicological properties, including endocrine disruption and potential carcinogenicity,[5] neural toxicity[6] and immunotoxicity,[7] have aroused increasing environmental and public health concerns. It was added to the list of persistent organic pollutants (POPs) that need special consideration at the recent Stockholm convention.[8] Thus, it is vital to develop efficient treatment technology for PFOA elimination under mild conditions.

However, the C–F bond in the PFOA molecule has the strongest chemical bonding energy in nature (~110 kcal mol^{-1}), making it extremely difficult to degrade by conventional technologies.[9–11] The widely applied advanced oxidation process (AOP), which utilizes hydroxyl radicals ($^{\bullet}OH$) to attack refractory pollutants *via* hydrogen abstraction,[12–14] is also ineffective in degrading PFOA, because the carbon chain of PFOA has no hydrogen atoms to be abstracted.[15] Pulse radiolysis studies have also confirmed that perfluorinated compounds are practically unreactive towards $^{\bullet}OH$.[16] Although several oxidative methods, including sulfate radical oxidation,[17–19] photocatalytic oxidation,[20] sonochemical degradation[21] and electrolysis,[22] have been reported to degrade perfluorinated acids, the defluorination efficiencies are rather low and the use of these methods

Guangdong Key Laboratory of Environmental Catalysis and Health Risk Control, Guangzhou Key Laboratory of Environmental Catalysis and Pollution Control, School of Environmental Science and Engineering, Institute of Environmental Health and Pollution Control, Guangdong University of Technology, Guangzhou 510006, China. E-mail: antc99@gdut.edu.cn; Fax: +86 20 3932 2298; Tel: +86 20 3932 2298

† Electronic supplementary information (ESI) available. See DOI: 10.1039/d0ew00205d

requires not only strict reaction conditions but also high energy consumption.

In this regard, photochemical methods using solar energy have attracted increasing interest as sustainable and environmentally benign technologies for PFOA treatment. However, most photochemical processes are also based on almost exclusively oxidative reactions,[23–25] in which the defluorination efficiency for PFOA and its intermediates is still not satisfactory. Fortunately, it is known that the F atom has the highest electronegativity among all elements, and its strong electron withdrawing ability enables the F atom to act as a reductive reaction center for defluorination *via* nucleophilic agent attack. For example, Huang *et al.*[26] showed the feasibility of the reaction between hydrated electrons (e_{aq}^-) and perfluorinated acids using the laser flush photolysis of $K_4Fe(CN)_6$ in water. The reductive degradation rate constants are increased with increasing CF_2 chain length, suggesting that the F atom is the reductive center. Therefore, several reductive agents including I^-,[27,28] sulfite[29] and oxalic acid[30] have been utilized to treat PFOA *via* photo-reductive pathways with high defluorination efficiency. However, these methods all require UV irradiation as the light source, which contains only 5% of solar energy. The defluorination of perfluorinated acids by using visible light (~45% of solar energy) *via* photo-reductive technologies still remains a mystery.

To achieve defluorination of PFOA under visible light (VL) irradiation, one of the major tasks was to develop narrow band gap photocatalysts which can use VL energy well. However, a narrow band gap usually leads to the fast recombination of excitons. This problem may be potentially solved by adding external electron donors to trap photo-generated h^+, thus facilitating the separation of charge carriers so that more photo-generated e^- can be used for PFOA reductive degradation. In addition, noble metal (*i.e.* Pt) loading has been proven to be an effective way to further accelerate interfacial electron transfer.[31] Therefore, high defluorination efficiency under VL may be achieved by combining a narrow band gap photocatalyst with electron donors and Pt loading. To this end, monoclinic dibismuth tetraoxide (Bi_2O_4) has been recently found to be a novel and good photocatalyst with a wide VL absorption range up to 620 nm.[32] It has aroused great interest for applications in the degradation of refractory organic pollutants because of its excellent activity and facile green synthesis.[33–36] Its high VL absorption and suitable band structure could make it an attractive candidate for PFOA treatment under mild conditions.

Herein, VL-driven photo-reductive defluorination of PFOA was first attempted with addition of different electron donors and by using m-Bi_2O_4 with Pt loading as the representative photocatalyst to demonstrate the feasibility. The effect of different electron donors on the defluorination efficiency was also investigated in detail. The intermediates as well as the mass balance of fluorine during the degradation were investigated. Finally, a defluorination mechanism based on photo-reductive decomposition was also proposed. This work is expected to provide new strategies for PFOA treatment *via* reductive pathways based on well-designed novel photocatalysts under VL irradiation.

2. Experimental

2.1. Chemicals and synthesis

2.1.1. Chemicals. Sodium bismuthate ($NaBiO_3$, 99%), pentafluoropropionic acid (PFPrA, 97%), trifluoroacetic acid (TFA, 99%), perfluorobutyric acid (PFBA, 99%), perfluoroheptanoic acid (PFHpA, 99%), perfluorohexanoic acid (PFHxA, 97%), perfluoropentanoic acid (PFPeA, 94%), perfluorooctanoic acid (PFOA, 90%) as well as chloroplatinic acid (H_2PtCl_6, AR) were used as purchased without any further purification.

2.1.2. Synthesis of materials. Dibismuth tetraoxide (Bi_2O_4) was prepared using a simple hydrothermal method with $NaBiO_3$ as the only starting material based on published work.[32] Specifically, $NaBiO_3$ powder (0.56 g) was added into water and then placed into a 20 mL Teflon lined stainless steel autoclave, which was then sealed and heated under autogenous pressure in an oven set at 160 °C for 12 h. After collection with a centrifuge (5000 rpm), the final product was collected, and then cleaned with deionized water. Finally, the product was dried at 55 °C overnight. Pt-loaded Bi_2O_4 was obtained by using a photo-reduction method. Briefly, 16 mg Bi_2O_4 was dispersed in deionized water (20 mL) under stirring, followed by the addition of given amounts (0.5–2%) of H_2PtCl_6 solution. The suspension was then irradiated for 2 h with a xenon lamp. Finally, the products were collected, cleaned and dried overnight. The as-prepared samples were characterized using a series of techniques including SEM/TEM, XRD, UV-vis DRS, XPS and photoelectrochemical tests. The characterization details can be found in the ESI.†

2.2. Photocatalytic defluorination of PFOA

The degradation reaction was performed in a homemade quartz tube reactor with 30 mm inner diameter. Briefly, 16 mg Pt–Bi_2O_4 was dispersed in 80 mL PFOA solution (100 ppb). Then, different amounts of KI (1–9 mM) were added to the mixture under vigorous stirring. Prior to starting the light irradiation, N_2 was bubbled through the mixture for 0.5 h to remove O_2 from the solution. The suspension was illuminated with a 300 W xenon lamp equipped with a 420 nm cut-off filter ($\lambda > 420$ nm). The light intensity was fixed at 100 mW cm^{-2}. At certain time intervals, aliquots of the suspension were taken from the reactor and filtered through a nylon filter (0.22 mm) (Millipore) before measurement. During the reaction, the temperature was maintained at 25 °C by water circulation. The pH was adjusted with 0.1 M HCl or NaOH. For comparison, the electron donors Na_2SO_3, Na_2S and vitamin C were also used for tests under identical conditions. All the experiments were performed in triplicate.

2.3. Analytical methods

PFOA concentrations and possible intermediates were analyzed with HPLC-MS/MS (Q Exactive, Thermo, USA) with a Hypersil GOLD C18 column (100 × 2.1 mm, 1.9 μm). Thermo Scientific Xcalibur and Compound Discover were used for the data acquisition and processing. The employed mobile phase was composed of 0.1% formic acid aqueous solution (solvent A) and methanol (solvent B), starting at 2% methanol for 2 min, and then increasing linearly. The gradient increased to 95% methanol at 15 min, and was maintained until 18 min before reversion to the original conditions. The injection volume was 1 μL and the flow rate was set to 0.25 mL min^{-1}. Full MS mode was used and the scan range was 100–1000 *m*/*z*. The *m*/*z* values are shown in Table S1.† During the PFOA degradation processes, the released F^- concentrations were analyzed using ion chromatography (761 compact IC, Metrohm, Switzerland). A Metrosep Supp 5 column (150 mm × 4.0 mm) with a Metro A Guard column (5 mm × 4.0 mm) was used for the analysis of F^- concentrations. A mixed solution of Na_2CO_3 (3.2 mmol L^{-1}) and $NaHCO_3$ (1 mmol L^{-1}) was used as a mobile phase for F^- concentration analysis with a flow rate set at 0.7 mL min^{-1}. During the photocatalytic reduction process, the defluorination efficiency was calculated using eqn (1):

$$\text{Defluorination efficiency} = C_F/(C_0 \times 15) \times 100\% \quad (1)$$

In this equation, C_F is the concentration of F^- released during the photocatalytic reduction process; C_0 represents the initial concentration of PFOA before the reaction; and "15" is the number of F atoms in the PFOA molecule.[20]

3. Results and discussion

3.1. Material characterization

Using X-ray diffraction (XRD) technology, the crystal structure of the prepared samples was characterized. As shown in Fig. 1a, the XRD pattern of Bi_2O_4 could be well indexed to the monoclinic phase of Bi_2O_4 (JCPDS-830410) without other impurities. In addition, after loading with Pt nanoparticles, the obtained Pt–Bi_2O_4 exhibits a similar XRD pattern to Bi_2O_4, probably due to the low doping content of Pt, which also suggests that the Pt nanoparticles are highly dispersed on the Bi_2O_4 surface. The UV-vis DRS spectra in Fig. 1b confirm that the as-prepared Bi_2O_4 has high VL absorption with a cut-off wavelength of up to 620 nm, which is consistent with our previous study.[32] Pt–Bi_2O_4 exhibits slightly enhanced VL absorption, suggesting that Pt loading could also improve the VL absorption of Bi_2O_4.

The scanning electron microscopy (SEM) image demonstrates that Pt–Bi_2O_4 has a nanorod morphology (Fig. S1a†). The transmission electron microscopy (TEM) image further confirms that nanorods with length of 1.7 μm and diameter of 610 nm were obtained (Fig. S1b†). The clear lattice fringes with d = 0.332 nm match well with the (111) crystal plane of Bi_2O_4 (Fig. S1c†). The loaded Pt nanoparticles were not obvious and were difficult to locate. However, their existence could be verified by the EDS spectrum, which clearly demonstrates the presence of Bi, O and Pt elements in the catalyst (Fig. S1d†). The Cu signal originated from the conducting substrate. The HAADF and corresponding elemental mapping analysis (Fig. S1e†) further demonstrate the existence and distribution of these elements, with the Pt amount determined to be 0.36%, which is close to the theoretical value of 0.50%. These results confirm the successful photo-reduction synthesis of Pt–Bi_2O_4 with ultrafine Pt nanoparticles highly dispersed on the catalyst surface.

3.2. Photocatalytic defluorination of PFOA

Visible light-driven decomposition of PFOA was carried out by using a xenon lamp with an optical cut-off filter ($\lambda > 420$ nm) as a light source. Spectral analysis of the light confirms that there is no UV light irradiation (Fig. S2†). The light control (without photocatalyst) experiments indicate that PFOA is stable under VL irradiation, while dark control (without light irradiation) experiments show that Pt–Bi_2O_4/KI

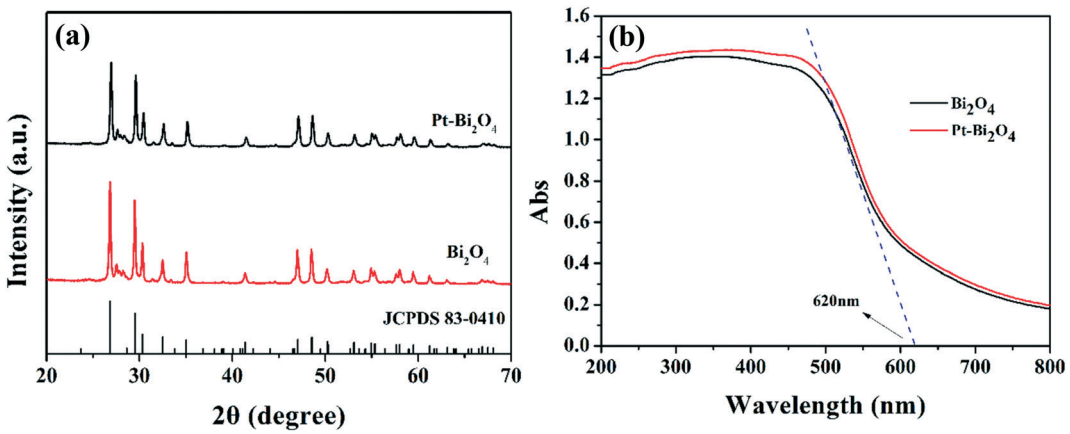

Fig. 1 (a) X-ray diffraction (XRD) patterns and (b) UV-vis diffuse reflectance spectra (UV-vis DRS) of the as-prepared Bi_2O_4 and Pt–Bi_2O_4 samples.

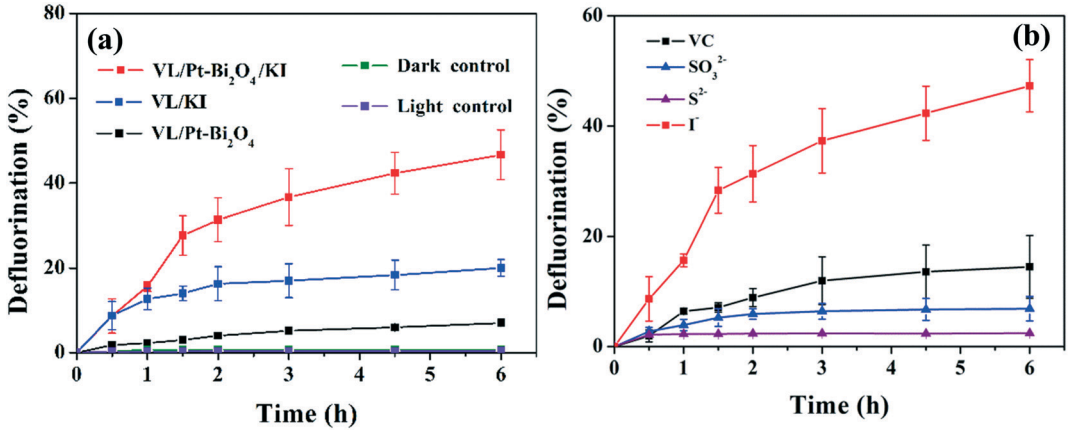

Fig. 2 (a) Photocatalytic defluorination efficiency of perfluorooctanoic acid (PFOA) by the as-prepared samples under different conditions; (b) photocatalytic defluorination efficiency with several different electron donors. Experimental conditions: [PFOA] = 100 ppb; [catalyst] = 200 mg L^{-1}; [I^-, SO_3^{2-}, S^{2-}, vitamin C] = 6 mM; $\lambda > 420$ nm; T = 25 °C.

is also ineffective for PFOA decomposition under dark conditions (Fig. 2a). It was found that the defluorination of PFOA was only about 7% after 6 h of VL irradiation in the presence of Pt–Bi_2O_4 alone, due to the narrow band gap of Bi_2O_4 which led to fast photo-generated charge recombination. Interestingly, the addition of 6 mM KI could dramatically promote the decomposition process and the defluorination efficiency reached 44% within 6 h, nearly 9.0 times higher than that without KI addition. The defluorination efficiency was significantly decreased to only about 20% in the absence of Pt–Bi_2O_4, suggesting that the contributions of both Pt–Bi_2O_4 and KI as the electron donor are crucial for the efficient decomposition of PFOA. To further study the effect of other electron donors, several typical reducing agents including SO_3^{2-}, S^{2-} and vitamin C were also used. As shown in Fig. 2b, the introduction of SO_3^{2-} and S^{2-} has a very limited promoting effect, while vitamin C shows a moderate effect with a defluorination efficiency of 18.7%. Therefore, KI was found to be the optimal electron donor for PFOA decomposition. Previous studies have shown that SO_3^{2-} and S^{2-} were often used as electron donors for photocatalytic H_2 production, especially when using sulfides as the photocatalyst.[37,38] The standard redox potentials of S^{2-}/S_2^{2-} (−0.52 V) and $SO_3^{2-}/S_2O_6^{2-}$ (−0.25 V) are more negative than that of H^+/H_2,[39] and therefore H_2 may be produced in a competing side reaction which leads to a decrease in PFOA defluorination efficiency. The redox potentials of I^-/I_3^- and vitamin C are reported to be +0.54 V (ref. 39) and +0.35 V,[40] respectively, and so they are unable to produce H_2. Therefore, I^- and vitamin C are more efficient than SO_3^{2-} and S^{2-} as electron donors for PFOA defluorination. In addition, the inorganic I^- is probably more easily adsorbed onto Pt–Bi_2O_4 than the organic vitamin C, because I^- has a high affinity with Bi oxides to form oxyhalides.[41] This facilitates the trapping of photo-generated h^+ by I^- at the catalyst surface, which leads to its higher efficiency as an electron donor than that of vitamin C.

To probe whether the defluorination process occurs by an oxidation or reduction pathway, experiments were also conducted under different atmospheres (*i.e.* O_2 bubbling, N_2 bubbling and air equilibrium). Fig. 3a shows that under normal ambient conditions, the defluorination efficiency was only about 24% after 6 h of VL irradiation, and this value further decreased to 9% with O_2 bubbling, suggesting that the reaction would not proceed *via* an oxidation pathway. In contrast, the defluorination efficiency was increased to 44% on purging with N_2, which indicates that the reaction may proceed *via* a reduction pathway, because the removal of O_2 could inhibit the trapping of photo-generated e^- by dissolved O_2, facilitating direct electron transfer to PFOA molecules. To further investigate the role of KI as electron donor, experiments were conducted with the addition of different amounts of KI. It is clearly shown in Fig. 3b that the defluorination efficiency increased with increasing KI concentration. When the KI concentration was increased to 6 mM, the defluorination efficiency reached the highest value of 45% within 6 h, while on further increasing the KI concentration to 9 mM, the defluorination efficiency did not exhibit a significant difference. This may be due to the increase in triiodide (I_3^-) concentration at high concentrations of KI. In addition, iodide radicals ($I^{\cdot}$) could be generated during iodide anion photolysis. The iodide radical ($I^{\cdot}$) would then transform into triiodide (I_3^-) through a series of reactions, and triiodide could consume a larger amount of e^-, leading to a decrease in defluorination efficiency.[27]

Subsequently, the effect of Pt loading on the defluorination process was also studied. As shown in Fig. 3c, the defluorination efficiency first increases when the Pt loading amount is increased from zero to 0.5%, and then decreases when the Pt loading amount is further increased to 2%. The optimal Pt loading amount was determined to be 0.5%, which is similar to the amount used in previous studies for typical photochemical reduction reactions, such as H_2 production.[42] This result confirms the crucial role of Pt as co-catalyst for PFOA reduction. However, an excess loading amount would cause aggregation of the Pt nanoparticles covering the Bi_2O_4 surface, resulting in changes in the

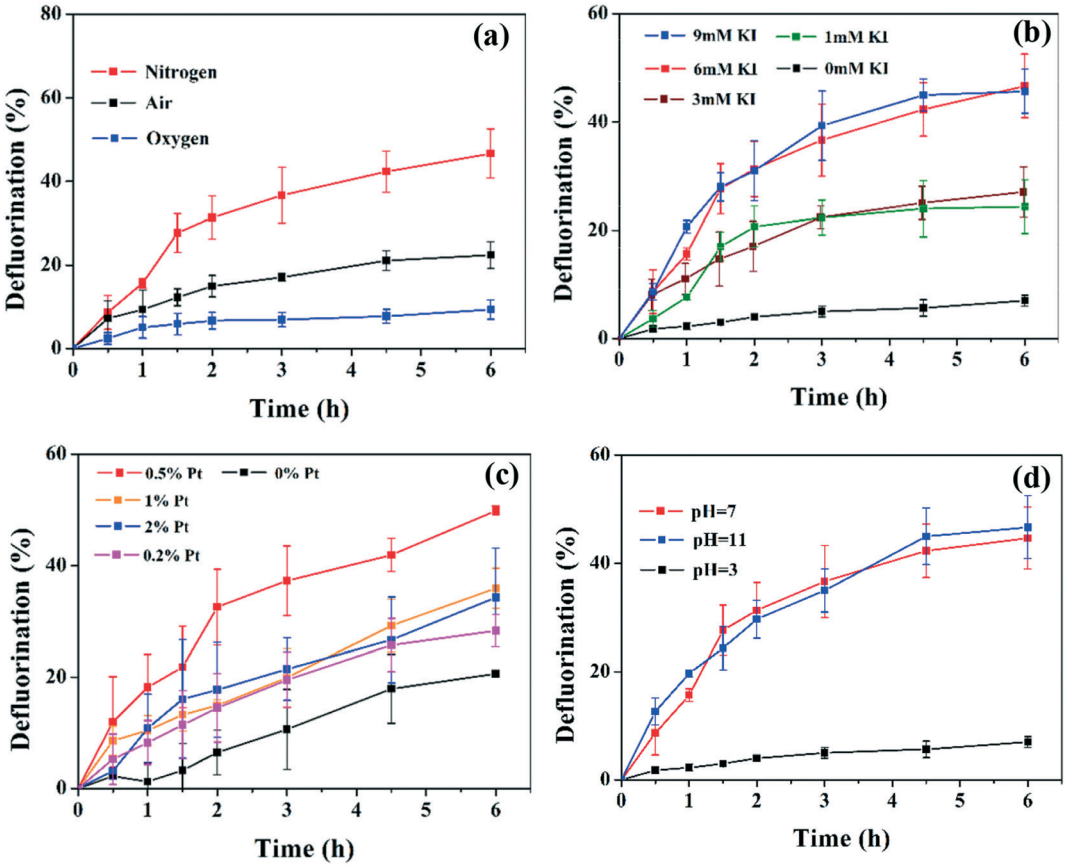

Fig. 3 (a) Photocatalytic PFOA defluorination efficiency under different atmosphere (O_2, N_2, air); (b) KI concentration (0–9 mM); (c) loading amount of Pt (0–2%); (d) pH value (3–11). Experimental conditions: [PFOA] = 100 ppb; [catalyst] = 200 mg L^{-1}; $\lambda > 420$ nm; T = 25 °C.

surface properties of Bi_2O_4 and the active reduction sites. In addition, the shielding effect of excess Pt could inhibit the absorption of light, further decreasing the activity. Nevertheless, these results confirm that both KI acting as an electron donor and Pt loading are crucial factors for the successful decomposition of PFOA on a Bi_2O_4 catalyst under VL irradiation.

It was further found that the pH had a significant influence on the defluorination efficiency. Fig. 3d shows that acidic conditions (pH = 3) could inhibit the reaction process, and the defluorination efficiency increased with an increase in pH value up to 11. This could be explained by two aspects. Firstly, the photo-generated e^- could react with H^+ under low pH conditions to produce $^{\cdot}H$, which leads to the quenching of photo-generated e^- under acidic conditions. Secondly, high pH values could promote the disproportionation of I_2 into I^- and IO_3^- ($3I_2 + 6OH^- \rightarrow 5I^- + IO_3^- + 3H_2O$), and therefore more I^- could be recycled and used for h^+ trapping reactions, leading to the enhanced separation of photo-generated e^-–h^+ pairs. Thus, more photo-generated e^- could be used for reduction of PFOA at high pH values. Similar results have also been found in a previous study which shows that the reductive defluorination of PFOA could be enhanced by increasing the pH value.[43] Nevertheless, these results indicate that the present system can work in a wide pH range of 5–11, which shows potential for practical applications.

3.3. Defluorination intermediates

To explore the defluorination process and mechanism, the degradation profile of PFOA was investigated. As Fig. 4a shows, the PFOA concentration decreased rapidly within the first 1 h, and the degradation efficiency reached about 45% within 6 h under VL irradiation. It was noted that the degradation efficiency was reduced significantly after the first 1 h, which was probably due to the formation of perfluorinated intermediates which could occupy the reaction centers on the catalyst surface, leading to a decrease in reaction kinetics.

The possible shorter chain perfluorocarboxylic acid (PFCA) intermediates with 2 to 7 carbon atoms were further determined using HPLC/MS. As Fig. 4b and Table S1† show, degradation intermediates including PFHpA ($C_6F_{13}COOH$, C7), PFHxA ($C_5F_{11}COOH$, C6), PFPeA (C_4F_9COOH, C5), PFBA (C_3F_7COOH, C4) and PFPrA (C_2F_5COOH, C3) were detected, which indicates that the C–C bonds are simultaneously cleaved during the photocatalytic reductive process. The concentrations of shorter chain PFCAs increased at the initial stage and then dropped with prolonged reaction time,

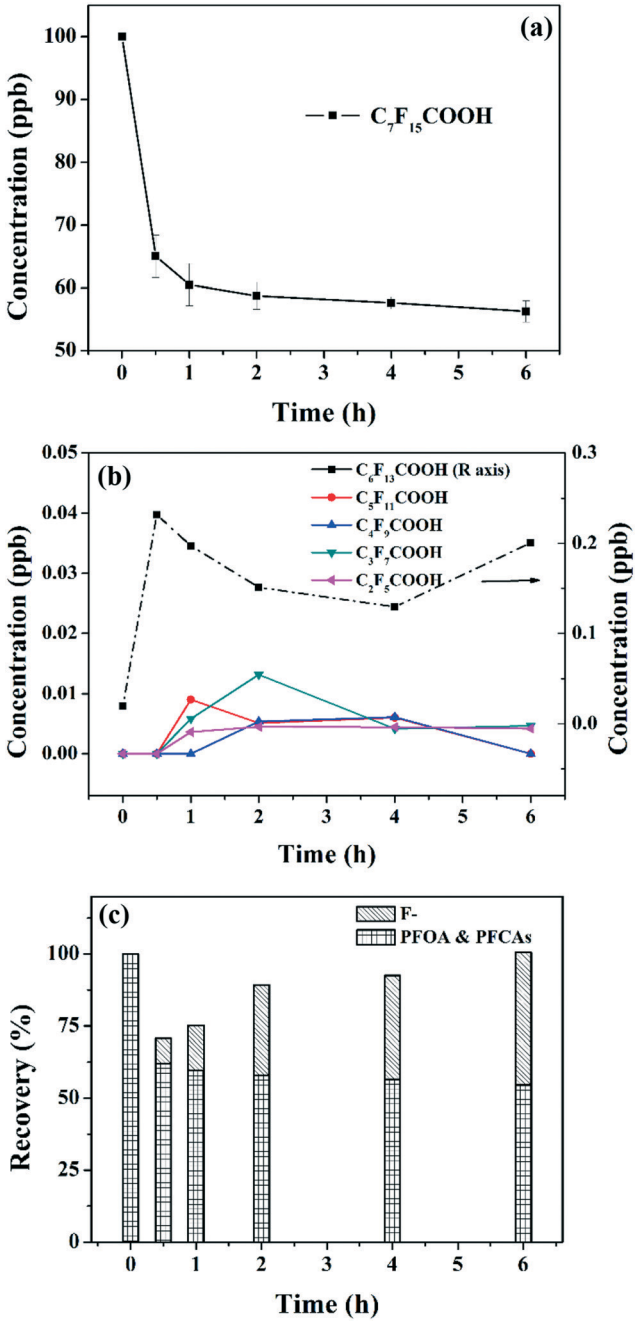

Fig. 4 Irradiation–time dependence profiles for (a) PFOA, (b) short-chain PFCAs detected by HPLC/MS, and (c) fluorine element mass balance during the photocatalytic defluorination process. Experimental conditions: [PFOA] = 100 ppb; [catalyst] = 200 mg L^{-1}; [KI] = 6 mM; $\lambda >$ 420 nm; T = 25 °C.

suggesting that these intermediates could be further decomposed. It was noted that the reaction times needed to reach the maximum concentrations of the intermediates were different, and were 0.5, 1 and 1.5 h for C7, C6 and C5, respectively, and 2 h for C4/C3. This indicated that PFOA as well as its intermediates were degraded step by step with loss of the carbon chain. As demonstrated, the C6 content was higher than the shorter chain (C3–C5) content at a reaction time of 1 h. On prolonging the reaction time to 2 h, the concentration of C6 became lower than that of C5 and C4. At a time of 6 h, the concentrations of C6 and C5 were zero, while there were still considerable amounts of C4 and C3. It was also noted that C7 was the main intermediate during the whole degradation process, since its concentration was the highest among all the intermediates. In addition, the amount of C7 increased rapidly in the initial stage (0–0.5 h) and decreased gradually in the middle stage (0.5–4 h), suggesting that C7 was generated first and underwent rapid decomposition to form shorter chains. However, the concentration of C7 increased again in the late stage (4–6 h), which indicates that the decomposition of C7 was inhibited, probably because the main event in the late stage was the decomposition of shorter chains. It has been reported that PFCAs with shorter chains are more difficult to degrade than longer chains, because shorter C–F chains would provide fewer attacking sites.[26,44] This may account for the decreased defluorination efficiency at the late stage with the formation of shorter chains. Besides the fully fluorinated carboxylic acids, less fluorinated carboxylic acids including $C_7F_{13}H_2COOH$, $C_7F_{14}HCOOH$, $C_6F_{12}HCOOH$ and $C_6F_{11}H_2$-COOH were also detected (Fig. S3†), which was also found in a previous study.[29]

Fig. 4c further demonstrates the fluorine mass balance during the process. At the beginning, all the F element was present in the carbon chain of PFOA. The total recovery of fluorine (that is, the molar ratio of the total fluorine content in F^-, residual PFOA and short-chain PFCAs to that in PFOA before reaction) was about 99% after 6 h of irradiation but only about 75% at the early stage within 1 h of VL irradiation. This demonstrates that additional fluorine-containing species, likely less fluorinated carboxylic acids such as $C_7F_{13}H_2COOH$ and $C_7F_{14}HCOOH$, could be formed during PFOA decomposition, especially at the beginning of the degradation. As time went by, these additional products were also further decomposed into F^-. These results suggest that many additional intermediates other than the original PFCAs could be formed in the VL/Pt–Bi_2O_4/KI system, but these intermediates could also be decomposed after prolonged reaction time in this system.

3.4. Photocatalytic reductive defluorination mechanism

To investigate the effect of Pt loading on the photocatalytic properties of the Bi_2O_4 photocatalyst, the photocurrent response was measured. Fig. 5a shows the average photocurrent density under VL irradiation. The Pt–Bi_2O_4 composite electrode displayed a photocurrent density of 0.5 μA cm^{-2}, which is 3.3 times higher that of the Bi_2O_4 electrode (0.15 μA cm^{-2}) under the same conditions. The EIS Nyquist plots of Bi_2O_4 sample electrodes with and without Pt loading were compared and the results are shown in Fig. 5b. The arc radius can act as an indicator to estimate the charge transfer efficiency on the electrodes.[45,46] Smaller radius indicates higher charge separation and migration efficiency. It was

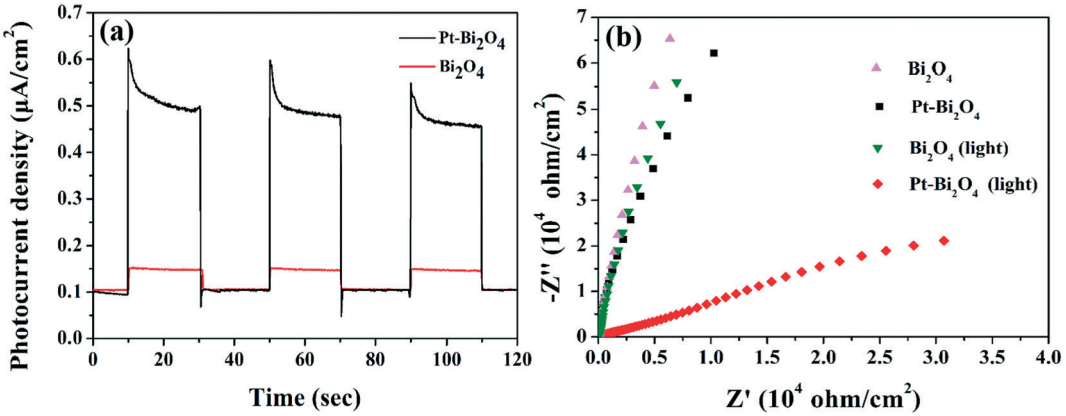

Fig. 5 (a) Transient photocurrent responses under VL irradiation and (b) electrochemical impedance spectroscopy (EIS) Nyquist plots for Bi_2O_4 and Pt–Bi_2O_4 (*Z*′: real impedance; *Z*″: imaginary impedance).

found that the arc radius of Pt–Bi_2O_4 was much smaller than that of Bi_2O_4 under both dark and light conditions, indicating that the charge separation as well as the migration of photo-generated e^-–h^+ pairs could be promoted by Pt loading, which agrees with the data of the photocurrent analysis. Our data also confirms that the photo-induced interface charge separation could be enhanced during the defluorination of PFOA by the surface Pt loading, which

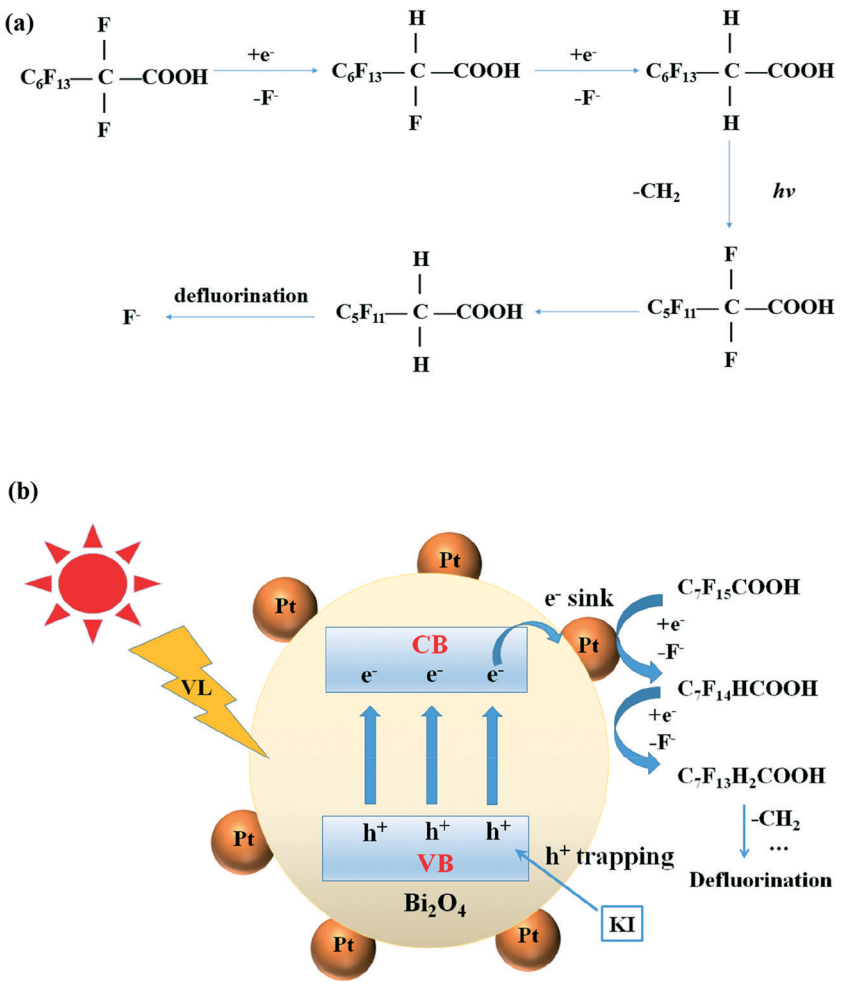

Fig. 6 (a) Possible photo-induced reductive defluorination pathway of PFOA; (b) schematic illustration of photocatalytic defluorination of PFOA in the VL/Pt–Bi_2O_4/KI system. CB: conduction band; VB: valance band.

functions as an electron sink to trap photo-generated e^-, thus promoting the photo-reductive defluorination of PFOA under VL irradiation.

Based on the above discussion, the dominant reactive species for the defluorination of PFOA are the photo-generated e^- formed during this process. Because of their high e^- affinity, the e^- firstly approach and attack the F atoms at the α-position, which means replacing a F atom with a H atom, resulting in the step by step decomposition of PFOA (Fig. 6a). This explains the fact that less fluorinated carboxylic acids (*i.e.* $C_7F_{13}H_2COOH$ and $C_7F_{14}HCOOH$) were found within the initial reaction period of 1 h. The content of $C_7F_{13}H_2COOH$ was lower than that of $C_7F_{14}HCOOH$, according to the chromatogram peak height (Fig. S3†). The produced $C_7F_{13}H_2COOH$ was further transformed into $C_6F_{13}COOH$ *via* the following reactions (eqn (2) and (3)) to remove a CF_2 unit:[29]

$$C_7F_{13}H_2COOH \rightarrow {}^{\bullet}C_6F_{13} + :CH_2 + {}^{\bullet}COOH \quad (2)$$

$${}^{\bullet}C_6F_{13} + {}^{\bullet}COOH \rightarrow C_6F_{13}COOH \quad (3)$$

Then, the produced $C_6F_{13}COOH$ was further degraded into $C_6F_{12}HCOOH$ and $C_6F_{11}H_2COOH$, losing a CF_2 unit to produce $C_5F_{11}COOH$ *via* a similar pathway. Finally, complete defluorination was achieved by stepwise removal of the CF_2 chain. Based on the above results, the overall defluorination mechanism is shown in Fig. 6b. Under VL irradiation, the Bi_2O_4 absorbs photons to generate e^-–h^+ pairs. The photo-generated e^- transfer to the Pt nanoparticles to react with PFOA molecules, which are defluorinated *via* a series of reductive reactions (Fig. 6a), while KI was used as the electron donor to accelerate the whole reaction process. It should be noted that prior studies have shown that hydrated electrons (e_{aq}^-) generated under UV irradiation are highly reactive in the defluorination of PFOA,[47,48] and the defluorination efficiency can be enhanced by a potential-driven electron transfer process.[47] Thus, there may be a possibility of potential-driven electron transfer from the catalyst surface, resulting in the formation of e_{aq}^- during the photocatalytic process even under VL irradiation, which needs future investigation.

3.5. Photostability of the reaction

To further investigate the photocatalyst stability in the VL/Pt–Bi_2O_4/KI system, recycling runs were also conducted. As shown in Fig. 7a, the defluorination efficiency remained

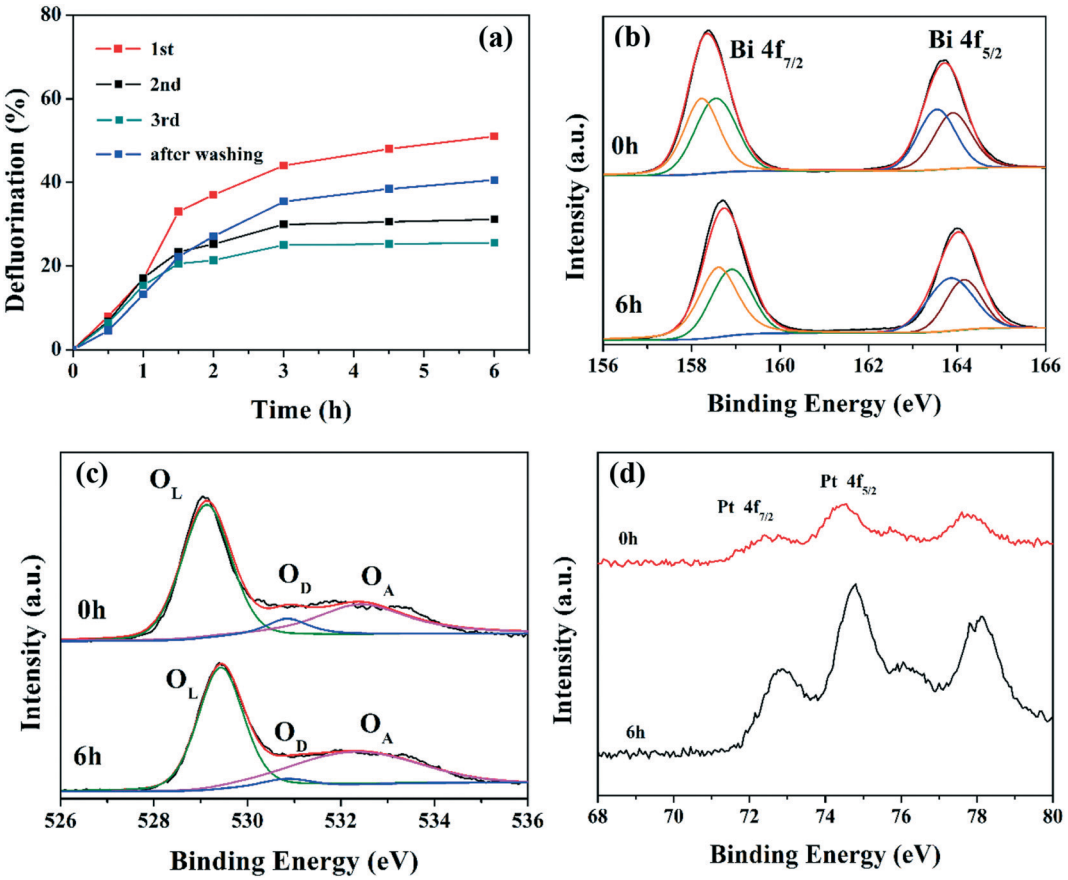

Fig. 7 (a) Repeated defluorination efficiency in the VL/Pt–Bi_2O_4/KI system; (b) X-ray photoelectron spectroscopy (XPS) high-resolution Bi 4f spectra; (c) O 1s spectra (O_L: crystal lattice oxygen; O_D: crystal defect lattice oxygen; O_A: adsorbed oxygen species); and (d) Pt 4f spectra of Pt–Bi_2O_4 before and after the defluorination reactions.

largely stable after three repeated experiments. There was a slight decrease in the efficiency after the 2nd and 3rd runs, probably due to surface adsorption of defluorination intermediates or loss of the photocatalyst during each recycling run. To confirm this, the used Pt–Bi_2O_4 photocatalyst was simply cleaned several times with distilled water and ethanol, and the defluorination efficiency was found to recover, suggesting that the photocatalyst was stable and the interactions between the catalyst and the intermediates were rather weak.

The stability of the catalyst was further verified by XPS measurements. The survey scan spectra show the presence of Bi, O, and Pt without other elements during the degradation process (Fig. S4†), suggesting that the photocatalyst surface was clean and no F-containing intermediates were adsorbed on the surface. The Bi $4f_{7/2}$ and Bi $4f_{5/2}$ peaks of pristine Bi_2O_4 were located at the binding energies of 158.7 and 163.6 eV, respectively, with a peak splitting of 4.9 eV (Fig. 7b). The Bi 4f peaks were found to shift to higher binding energy after 6 h degradation, suggesting that the surface ratio of Bi(v) to Bi(III) increased slightly after the reaction, which was attributed to oxidation by *in situ* photo-generated h^+ based on a previous study.[49] The O 1s spectra were deconvoluted into three peaks (Fig. 7c). The peak at binding energy 529.8 eV was ascribed to crystal lattice oxygen (defined as O_L); the peak at 531.1 eV was ascribed to lattice defect oxygen (O_D); and the one at 532.4 eV corresponds to the adsorbed oxygen species (O_A). The O_D/O_L ratio decreased from 0.15 to 0.05 after the degradation, indicating that the surface oxygen defects were gradually eliminated during the reaction, which inhibited the chemical adsorption of PFOA degradation intermediates and maintained the clean catalyst surface. The Pt 4f spectra also indicated that Pt^0 species were present during the degradation (Fig. 7d), further confirming the role of Pt loading. All these suggest that the present VL/Pt–Bi_2O_4/KI system is very stable during the degradation time period, which shows the potential application of this kind of sustainable and "green" technology in the elimination of PFOA in water.

Conclusions

In summary, a new visible light-induced PFOA defluorination strategy using Pt–Bi_2O_4 as a photocatalyst and KI as an electron donor was proposed. After 6 h of VL irradiation, the degradation efficiency could reach 45% and a defluorination efficiency of 44% was achieved. The defluorination mechanism was found to be a photocatalytic reduction process, in which the photo-generated e^- played the most important role. The Pt served as a co-catalyst to trap photo-generated e^-, while KI could trap photo-generated h^+ to suppress the undesired e^-–h^+ recombination, which cooperatively enhanced the defluorination efficiency. This work is expected to provide useful information for sustainable and "green" treatment of PFOA under mild conditions using solar energy, which may also have applications in the elimination of various refractory organic pollutants.

Conflicts of interest

The authors declare that they have no conflict of interest.

Acknowledgements

This work was supported by the National Natural Science Foundation of China (41425015 and 21607028), Science and Technology Project of Guangdong Province, China (2017A050506049), Local Innovative and Research Teams Project of Guangdong Pearl River Talents Program (2017BT01Z032), and Leading Scientific, Technical and Innovation Talents of Guangdong Special Support Program (2016TX03Z094).

Notes and references

1 Z. Wei, T. Xu and D. Zhao, Treatment of per- and polyfluoroalkyl substances in landfill leachate: status, chemistry and prospects, *Environ. Sci.: Water Res. Technol.*, 2019, **5**, 1814–1835.
2 M. Murakami, E. Imamura, H. Shinohara, K. Kiri, Y. Muramatsu, A. Harada and H. Takada, Occurrence and sources of perfluorinated surfactants in rivers in Japan, *Environ. Sci. Technol.*, 2008, **42**, 6566–6572.
3 C. A. Moody, J. W. Martin, W. C. Kwan, D. C. G. Muir and S. C. Mabury, Monitoring perfluorinated surfactants in biota and surface water samples following an accidental release of fire-fighting foam into Etobicoke Creek, *Environ. Sci. Technol.*, 2002, **36**, 545–551.
4 L. Ahrens, J. P. Benskin, I. T. Cousins, M. Crimi and C. P. Higgins, Themed issues on per- and polyfluoroalkyl substances, *Environ. Sci.: Water Res. Technol.*, 2019, **5**, 1808–1813.
5 L. Benbrahim-Tallaa, B. Lauby-Secretan, D. Loomis, K. Z. Guyton, Y. Grosse, F. El Ghissassi, V. Bouvard, N. Guha, H. Mattock, K. Straif and W. Int Agency Res Canc Monograph, Carcinogenicity of perfluorooctanoic acid, tetrafluoroethylene, dichloromethane, 1,2-dichloropropane, and 1,3-propane sultone, *Lancet Oncol.*, 2014, **15**, 924–925.
6 M. Kmecick, M. C. V. da Costa, C. A. D. Ribeiro and C. F. Ortolani-Machado, Morphological evidence of neurotoxic effects in chicken embryos after exposure to perfluorooctanoic acid (PFOA) and inorganic cadmium, *Toxicology*, 2019, **427**, 152286.
7 Z. M. Dong, M. M. Bahar, J. Jit, B. Kennedy, B. Priestly, J. Ng, D. Lamb, Y. J. Liu, L. C. Duan and R. Naidu, Issues raised by the reference doses for perfluorooctane sulfonate and perfluorooctanoic acid, *Environ. Int.*, 2017, **105**, 86–94.
8 M. Trojanowicz, K. Bobrowski, B. Szostek, A. Bojanowska-Czajka, T. Szreder, I. Bartoszewicz and K. Kulisa, A survey of analytical methods employed for monitoring of Advanced Oxidation/Reduction Processes for decomposition of selected perfluorinated environmental pollutants, *Talanta*, 2018, **177**, 122–141.

9 C. S. Liu, C. P. Higgins, F. Wang and K. Shih, Effect of temperature on oxidative transformation of perfluorooctanoic acid (PFOA) by persulfate activation in water, *Sep. Purif. Technol.*, 2012, **91**, 46–51.
10 D. H. Huang, L. F. Yin and J. F. Niu, Photoinduced hydrodefluorination mechanisms of perfluorooctanoic acid by the SiC/graphene catalyst, *Environ. Sci. Technol.*, 2016, **50**, 5857–5863.
11 Z. Song, X. L. Dong, J. D. Fang, C. H. Xiong, N. Wang and X. M. Tang, Improved photocatalytic degradation of perfluorooctanoic acid on oxygen vacancies-tunable bismuth oxychloride nanosheets prepared by a facile hydrolysis, *J. Hazard. Mater.*, 2019, **377**, 371–380.
12 M. G. Antoniou, J. A. Shoemaker, A. A. De La Cruz and D. D. Dionysiou, Unveiling new degradation intermediates/pathways from the photocatalytic degradation of microcystin-LR, *Environ. Sci. Technol.*, 2008, **42**, 8877–8883.
13 F. B. Yao, Y. Zhong, Q. Yang, D. B. Wang, F. Chen, J. W. Zhao, T. Xie, C. Jiang, H. X. An, G. M. Zeng and X. M. Li, Effective adsorption/electrocatalytic degradation of perchlorate using Pd/Pt supported on N-doped activated carbon fiber cathode, *J. Hazard. Mater.*, 2017, **323**, 602–610.
14 A. Matilainen and M. Sillanpaa, Removal of natural organic matter from drinking water by advanced oxidation processes, *Chemosphere*, 2010, **80**, 351–365.
15 S. N. Wang, Q. Yang, F. Chen, J. Sun, K. Luo, F. B. Yao, X. L. Wang, D. B. Wang, X. M. Li and G. M. Zeng, Photocatalytic degradation of perfluorooctanoic acid and perfluorooctane sulfonate in water: A critical review, *Chem. Eng. J.*, 2017, **328**, 927–942.
16 E. Szajdzinska-Pietek and J. L. Gebicki, Pulse radiolytic investigation of perfluorinated surfactants in aqueous solutions, *Res. Chem. Intermed.*, 2000, **26**, 897–912.
17 H. Hori, Y. Nagaoka, M. Murayama and S. Kutsuna, Efficient decomposition of perfluorocarboxylic acids and alternative fluorochemical surfactants in hot water, *Environ. Sci. Technol.*, 2008, **42**, 7438–7443.
18 Y. C. Lee, S. L. Lo, J. Kuo and Y. L. Lin, Persulfate oxidation of perfluorooctanoic acid under the temperatures of 20–40 degrees C, *Chem. Eng. J.*, 2012, **198–199**, 27–32.
19 N. Remya and J. G. Lin, Current status of microwave application in wastewater treatment—A review, *Chem. Eng. J.*, 2011, **166**, 797–813.
20 Y. Y. Sun, G. Y. Li, W. J. Wang, W. Q. Gu, P. K. Wong and T. C. An, Photocatalytic defluorination of perfluorooctanoic acid by surface defective BiOCl: Fast microwave solvothermal synthesis and photocatalytic mechanisms, *J. Environ. Sci.*, 2019, **84**, 69–79.
21 C. D. Vecitis, H. Park, J. Cheng, B. T. Mader and M. R. Hoffmann, Kinetics and mechanism of the sonolytic conversion of the aqueous perfluorinated surfactants, perfluorooctanoate (PFOA), and perfluorooctane sulfonate (PFOS) into inorganic products, *J. Phys. Chem. A*, 2008, **112**, 4261–4270.
22 J. F. Niu, H. Lin, J. L. Xu, H. Wu and Y. Y. Li, Electrochemical mineralization of perfluorocarboxylic acids (PFCAs) by Ce-doped modified porous nanocrystalline PbO_2 film electrode, *Environ. Sci. Technol.*, 2012, **46**, 10191–10198.
23 X. Y. Li, P. Y. Zhang, L. Jin, T. Shao, Z. M. Li and J. J. Cao, Efficient photocatalytic decomposition of perfluorooctanoic acid by indium oxide and its mechanism, *Environ. Sci. Technol.*, 2012, **46**, 5528–5534.
24 W. L. Zhang, D. Q. Zhang and Y. N. Liang, Nanotechnology in remediation of water contaminated by poly- and perfluoroalkyl substances: A review, *Environ. Pollut.*, 2019, **247**, 266–276.
25 H. Hori, A. Yamamoto, E. Hayakawa, S. Taniyasu, N. Yamashita and S. Kutsuna, Efficient decomposition of environmentally persistent perfluorocarboxylic acids by use of persulfate as a photochemical oxidant, *Environ. Sci. Technol.*, 2005, **39**, 2383–2388.
26 L. Huang, W. B. Dong and H. Q. Hou, Investigation of the reactivity of hydrated electron toward perfluorinated carboxylates by laser flash photolysis, *Chem. Phys. Lett.*, 2007, **436**, 124–128.
27 Y. Qu, C. J. Zhang, F. Li, J. Chen and Q. Zhou, Photo-reductive defluorination of perfluorooctanoic acid in water, *Water Res.*, 2010, **44**, 2939–2947.
28 H. Park, C. D. Vecitis, J. Cheng, W. Choi, B. T. Mader and M. R. Hoffmann, Reductive defluorination of aqueous perfluorinated alkyl surfactants: Effects of ionic headgroup and chain length, *J. Phys. Chem. A*, 2009, **113**, 690–696.
29 Z. Song, H. Q. Tang, N. Wang and L. H. Zhu, Reductive defluorination of perfluorooctanoic acid by hydrated electrons in a sulfite-mediated UV photochemical system, *J. Hazard. Mater.*, 2013, **262**, 332–338.
30 Y. Wang and P. Y. Zhang, Photocatalytic decomposition of perfluorooctanoic acid (PFOA) by TiO_2 in the presence of oxalic acid, *J. Hazard. Mater.*, 2011, **192**, 1869–1875.
31 K. Matsubara, M. Inoue, H. Hagiwara and T. Abe, Photocatalytic water splitting over Pt-loaded TiO_2 (Pt/TiO_2) catalysts prepared by the polygonal barrel-sputtering method, *Appl. Catal., B*, 2019, **254**, 7–14.
32 W. J. Wang, X. Q. Chen, G. Liu, Z. R. Shen, D. H. Xia, P. K. Wong and J. C. Yu, Monoclinic dibismuth tetraoxide: A new visible-light-driven photocatalyst for environmental remediation, *Appl. Catal., B*, 2015, **176–177**, 444–453.
33 D. H. Xia and I. M. C. Lo, Synthesis of magnetically separable Bi_2O_4/Fe_3O_4 hybrid nanocomposites with enhanced photocatalytic removal of ibuprofen under visible light irradiation, *Water Res.*, 2016, **100**, 393–404.
34 Y. F. Jia, S. P. Li, H. Ma, J. Z. Gao, G. Q. Zhu, F. C. Zhang, J. Y. Park, S. Cha, J. S. Bae and C. Liu, Oxygen vacancy rich Bi_2O_4–Bi_4O_7–BiO_{2-x} composites for UV-Vis-NIR activated high efficient photocatalytic degradation of bisphenol A, *J. Hazard. Mater.*, 2020, **382**, 121121.
35 Y. Y. Ma, C. Q. Zhang, C. Y. Li, F. Qin, L. Wei, C. Y. Hu, Q. H. Hu and S. W. Duo, Nanoscaled Bi_2O_4 confined in firework-shaped TiO_2 microspheres with enhanced visible light photocatalytic performance, *Colloids Surf., A*, 2019, **580**, 123757.
36 J. Li, X. Y. Wu, Z. Wan, H. Chen and G. K. Zhang, Full spectrum light driven photocatalytic *in-situ* epitaxy of one-

unit-cell $Bi_2O_2CO_3$ layers on Bi_2O_4 nanocrystals for highly efficient photocatalysis and mechanism unveiling, *Appl. Catal., B*, 2019, **243**, 667–677.

37 W. Zhong, X. Huang, Y. Xu and H. G. Yu, One-step facile synthesis and high H_2-evolution activity of suspensible $Cd_xZn_{1-x}S$ nanocrystal photocatalysts in a S^{2-}/SO_3^{2-} system, *Nanoscale*, 2018, **10**, 19418–19426.

38 R. J. Yang, K. L. Song, J. S. He, Y. Y. Fan and R. S. Zhu, Photocatalytic hydrogen production by RGO/$ZnIn_2S_4$ under visible light with simultaneous organic amine degradation, *ACS Omega*, 2019, **4**, 11135–11140.

39 G. S. Zhang, W. Zhang, J. Crittenden, D. Minakata, Y. S. Chen and P. Wang, Effects of inorganic electron donors in photocatalytic hydrogen production over Ru/$(CuAg)_{0.15}In_{0.3}Zn_{1.4}S_2$ under visible light irradiation, *J. Renewable Sustainable Energy*, 2014, **6**, 033131.

40 T. Matsui, Y. Kitagawa, M. Okumura and Y. Shigeta, Accurate standard hydrogen electrode potential and applications to the redox potentials of Vitamin C and NAD/NADH, *J. Phys. Chem. A*, 2015, **119**, 369–376.

41 H. F. Cheng, B. B. Huang, Y. Dai, X. Y. Qin and X. Y. Zhang, One-step synthesis of the nanostructured AgI/BiOI composites with highly enhanced visible-light photocatalytic performances, *Langmuir*, 2010, **26**, 6618–6624.

42 F. L. Yang, Q. Zhang, L. Zhang, M. T. Cao, Q. Q. Liu and W. L. Dai, Facile synthesis of highly efficient Pt/N-rGO/N-$NaNbO_3$ nanorods toward photocatalytic hydrogen production, *Appl. Catal., B*, 2019, **257**, 117901.

43 Y. Qu, C. J. Zhang, P. Chen, Q. Zhou and W. X. Zhang, Effect of initial solution pH on photo-induced reductive decomposition of perfluorooctanoic acid, *Chemosphere*, 2014, **107**, 218–223.

44 H. T. Tian and C. Gu, Effects of different factors on photodefluorination of perfluorinated compounds by hydrated electrons in organo-montmorillonite system, *Chemosphere*, 2018, **191**, 280–287.

45 W. J. Wang, Y. C. Li, Z. W. Kang, F. Wang and J. C. Yu, A NIR-driven photocatalyst based on α-$NaYF_4$:Yb,Tm@TiO_2 core–shell structure supported on reduced graphene oxide, *Appl. Catal., B*, 2016, **182**, 184–192.

46 M. Wang, P. Y. Guo, Y. Zhang, C. M. Lv, T. Y. Liu, T. Y. Chai, Y. H. Xie, Y. Z. Wang and T. Zhu, Synthesis of hollow lantern-like Eu(III)-doped g-C_3N_4 with enhanced visible light photocatalytic performance for organic degradation, *J. Hazard. Mater.*, 2018, **349**, 224–233.

47 Y. M. Su, U. Rao, C. M. Khor, M. G. Jensen, L. M. Teesch, B. M. Wong, D. M. Cwiertny and D. Jassby, Potential-driven electron transfer lowers the dissociation energy of the C–F bond and facilitates reductive defluorination of perfluorooctane sulfonate (PFOS), *ACS Appl. Mater. Interfaces*, 2019, **11**, 33913–33922.

48 M. J. Bentel, Y. C. Yu, L. H. Xu, Z. Li, B. M. Wong, Y. J. Men and J. Y. Liu, Defluorination of per- and polyfluoroalkyl substances (PFASs) with hydrated electrons: Structural dependence and implications to PFAS remediation and management, *Environ. Sci. Technol.*, 2019, **53**, 3718–3728.

49 D. Wu, L. Q. Ye, S. T. Yue, B. Wang, W. Wang, H. Y. Yip and P. K. Wong, Alkali-induced *in situ* fabrication of Bi_2O_4-decorated BiOBr nanosheets with excellent photocatalytic performance, *J. Phys. Chem. C*, 2016, **120**, 7715–7727.

